Angewandte Chemie
Eine Zeitschrift der Gesellschaft Deutscher Chemiker

Supporting Information

Highly Emissive Self-Trapped Excitons in Fully Inorganic Zero-Dimensional Tin Halides

*Bogdan M. Benin[+], Dmitry N. Dirin[+], Viktoriia Morad, Michael Wörle, Sergii Yakunin, Gabriele Rainò, Olga Nazarenko, Markus Fischer, Ivan Infante, and Maksym V. Kovalenko**

anie_201806452_sm_miscellaneous_information.pdf

SUPPORTING INFORMATION

Table of Contents

1. EXPERIMENTAL PROCEDURES

1.1 Materials

Cesium bromide (CsBr, 99%), rubidium bromide (RbBr, 99.8%) were purchased from ABCR. Cesium bromide (CsBr, 99%) and tin (II) bromide ($SnBr_2$, 99.2%) were purchased from Alfa Aesar. Tin (II) iodide (SnI_2, 99%) was purchased from STREM Chemicals, Inc. Cesium iodide (CsI, 99.9%) was purchased from ACROS. Potassium bromide (KBr) and silver bromide (AgBr) were purchased from Fluka. Sodium bromide (NaBr, ≥99.5%) was purchased from Sigma.

All chemicals were stored and handled, and all manipulations were performed air-free and inside an Ar filled glovebox with H_2O and O_2 levels <0.1 ppm. All chemicals were used as received without further purification.

Pyrex tubes (DURAN®) were purchased from Schott AG (12.00 ± 0.16 mm outer diameter with 1.50 ± 0.07 mm thickness). These were made into ampules and sealed using an oxygen-hydrogen flame.

1.2 Synthesis of Cs_4SnBr_6

CsBr and $SnBr_2$ were mixed in a 4.5:1 molar ratio, mortared, and pressed together into a pellet (> 5 tons of pressure, 12 mm die). The pellet was then sealed under vacuum (10^{-2} – 10^{-3} mbar) in a Pyrex tube and heated to 350 °C for 60 hours. The tube was opened in the glovebox, and the above process was repeated once more. The previously reported pseudo-binary phase diagram shows that Cs_4SnBr_6 undergoes a peritectic decomposition when heated above 380°C. Accordingly, cooling a melt with this composition, the resulting product consists of a mixture of CsBr, $CsSnBr_3$, and Cs_4SnBr_6. Therefore, a phase pure synthesis of Cs_4SnBr_6 can only be achieved by annealing a solid mixture of CsBr and $SnBr_2$.

1.3 Synthesis of mixed cation and mixed anion $Cs_{4-x}A_xSn(Br_{1-y}I_y)_6$ (A = Rb, K; x ≤ 1, y ≤ 1)

The synthesis of mixed cation, mixed anion, or mixed cation and anion phases was conducted using the same general procedure as above. *For A-site substitution:* CsBr was replaced with RbBr or KBr. The total, molar quantity of Cs, Rb, and K was at least 4.5x that of Sn. *For X-site substitution:* iodide was introduced into the system by exchanging CsBr for CsI. In the case of Cs_4SnI_6, $SnBr_2$ was replaced with SnI_2. Briefly, mortared samples were pressed at pressures >5 tons in an Ar-filled glovebox, sealed in evacuated Pyrex tubes, and heated to 350 °C. This was repeated at least twice until a visually off-white material was obtained after grinding. Further heating is possible, but not necessary after this point. Single crystals were grown by subjecting a previously prepared sample of Cs_4SnBr_6 to additional heating cycles. The length of each heating cycle was extended to 100 hrs. Through this approach small crystals, 20-40 microns in size, were successfully grown.

1.4 Absorption, photoluminescence, and photoluminescence excitation spectra

The diffuse reflectance spectra of the microcrystalline powders were collected using a Jasco V670 spectrophotometer equipped with an integrating sphere (ILN-725). The absorption spectra were then calculated using a Kubelka-Munk transformation. The spectrophotometer has two lamps: a deuterium (D_2) lamp (190-350nm), and a halogen lamp (330-2700 nm). In a routine measurement, powder samples were kept between two quartz slides and the spectra were measured from 250–800 nm with the lamp change occurring at 330 nm.

Photoluminescence and photoluminescence excitation spectra were measured using a Fluorolog iHR 320 Horiba Jobin Yvon spectrofluorometer equipped with a Xe lamp and a photomultiplier tube. Samples were measured while held between quartz slides. Variable temperature spectra were measured in a Joule–Thomson cryostat (MMR Technologies) operated in the temperature range of 78-300 K. PL emission could be recorded with a heating rate of approximately 5 K/min. Absolute values of photoluminescence quantum yield (PLQY) were measured at Quantaurus-QY spectrometer from Hamamatsu in powder mode.

1.5 Time-resolved photoluminescence

Time-resolved photoluminescence (TRPL) traces were recorded with a 355 nm excitation source (a frequency-tripled, picosecond Nd:YAG laser, Duetto from Time-Bandwidth). Scattered laser emission was filtered out using dielectric long-pass filters with edges at 400 nm. Measurements were performed using a time-correlated single photon counting (TCSPC) setup, equipped with a SPC-130-EM counting module (Becker & Hickl GmbH) and an IDQ-ID-100-20-ULN avalanche photodiode (Quantique) for recording the decay traces. The average radiative lifetimes were determined as $\tau_{avg} = (\sum_{i=1}^{2} \tau_i^2 \cdot A_i) / (\sum_{i=1}^{2} \tau_i \cdot A_i)$ where A_i and τ_i are the corresponding amplitudes and exponential decay parameters in a bi-exponential analysis.

1.6 Low-temperature photoluminescence

Temperature-dependent PL spectra were obtained by exciting the sample with a 355 nm pulsed laser. The sample was mounted in a helium exchange cryostat and the PL was analyzed by a 0.5m monochromator coupled to a nitrogen-cooled CCD camera.

1.7 Powder diffraction and single crystal diffraction

Powder diffraction patterns were collected on a STADI P diffractometer (STOE & Cie GmbH, Darmstadt, Germany) in transmission mode (Debye-Scherrer geometry). The diffractometer is equipped with a silicon strip MYTHEN 1K detector (Fa. DECTRIS) and a curved Ge (111)-monochromator ($CuK\alpha_1$, λ=1.54056 Å).

Single-crystal X-ray diffraction measurements were conducted on an XtraLAB Synergy, Dualflex, Pilatus 300K diffractometer equipped with a PhotonJet (Cu) X-ray source (CuKα, λ=1.54184 Å; micro-focus sealed X-ray tube) and mirror monochromator. Crystals were tip-mounted on a micromount with paraffin oil. Absorption correction performed with Multi-scan *CrysAlis PRO* 1.171.39.31d (Rigaku Oxford Diffraction, 2017). Empirical absorption correction using spherical harmonics, implemented in SCALE3 ABSPACK scaling algorithm. Data was processed and refined with *CrysAlis PRO* 1.171.39.31d (Rigaku OD, 2017), *SHELXS*,[1] XL,[1] and Olex2.[2]

1.8 Scanning electron microscopy and energy-dispersive X-ray spectroscopy

Scanning electron microscopy (SEM) of the as-obtained sample was done on a Quanta 200F microscope (Thermo Fisher Scientific) operated at an acceleration voltage V_{acc} = 20 kV. Energy-dispersive X-ray spectroscopy (EDS) was performed with an Octane SDD detector (EDAX, Ametec) attached to the microscope column. For spectra recording and quantification (ZAF correction), the software Gemini (EDAX) was used.

2. RESULTS AND DISCUSSION

2.1 Structural and optical characterization

When measuring the powder pattern of polycrystalline samples obtained with shorter tempering time, no other phases except Cs_4SnBr_6 and CsBr were observed (when ratios of CsBr:$SnBr_2$ ≥ 4.5:1 are used). The powder pattern was measured at room temperature and refined using the General Structure Analysis System (GSAS) with EXPGUI and GSASII.[3] Weight fractions of 92.5% and 7.5% were found for Cs_4SnBr_6 and CsBr, respectively (reflections arising from CsBr are indicated by blue asterisks; Fig. S1, 2).

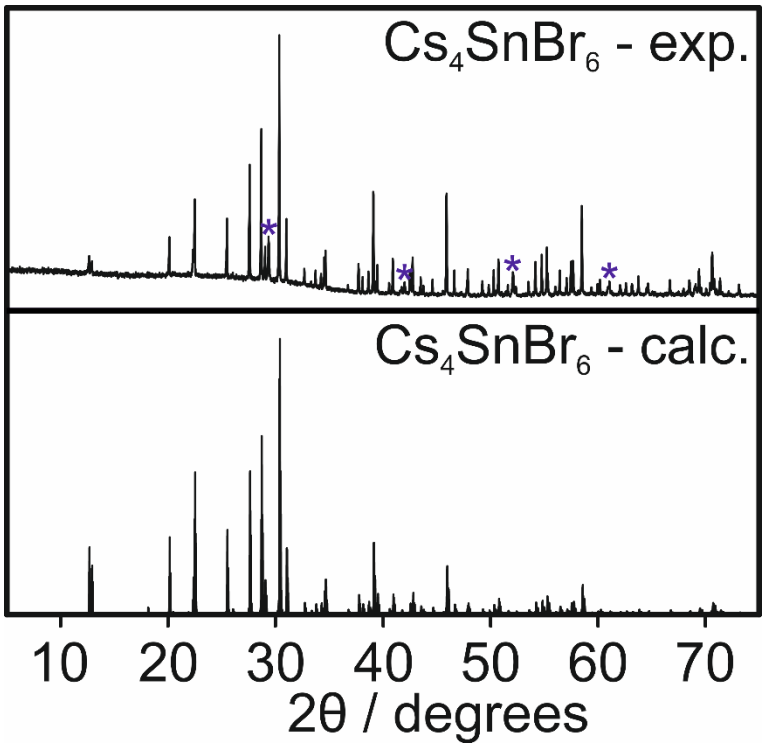

Figure S1. Experimental and calculated powder patterns of Cs_4SnBr_6. The experimental powder pattern collected from Cs_4SnBr_6 demonstrates that a typical reaction produces a majority of Cs_4SnBr_6 with a side product of CsBr (denoted by blue asterisks). This is expected given the slight excess of CsBr used in the initial reaction mixture. The Cs_4SnBr_6 diffraction pattern was calculated in Vesta3 using the experimentally determined structure of Cs_4SnBr_6.

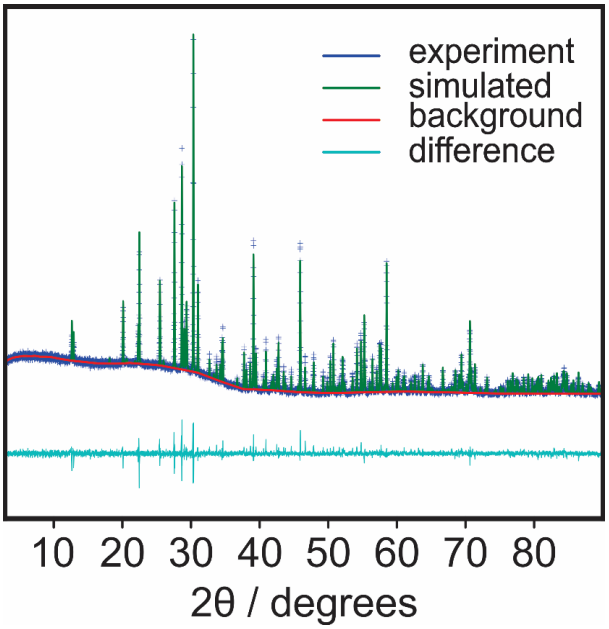

Figure S2. Refinement of Cs_4SnBr_6. The unit cell constants of Cs_4SnBr_6 at RT were determined through Rietveld refinement using GSASII.

Table S1. Refinement of Cs_4SnBr_6.

Sample	**Cs_4SnBr_6**
Temperature	298 K
Formula Weight	1129.73
Crystal System	trigonal
Space Group	*R-3c*
Color	Colorless
a (Å)	13.676354
c (Å)	17.271424
Volume (Å3)	2797.69
Z	6.0
F(000)	2880.0
ρ_{calc} (g cm^{-3})	4.023
Radiation	Cu Kα (λ = 1.54184 Å)
2θ for data collection (°)	3.03–90.02
2θ step (°)	0.01
Data/restraints/para-meters	8700/0/49
Rp	0.034
Rwp	0.046
Rexp	0.037
χ^2	1.610
Sample	Cs4SnBr6
Temperature	298 K

Table S2. Fractional atomic coordinates and isotropic or equivalent isotropic displacement parameters (Å^2) for Cs_4SnBr_6.

Atom	**Wyckoff Symbol**	**X**	**Y**	**Z**	**Uiso*/Ueq**
Sn1	*6b*	0	0	0	0.0199 (5)*
Cs1	*18e*	0.37525 (12)	0	1/4	0.0199 (5)*
Cs2	*6a*	0	0	1/4	0.0199 (5)*
Br1	*36f*	0.14145 (17)	0.50449 (19)	0.06624 (10)	0.0199 (5)*

Table S3. Variable temperature diffraction data for Cs_4SnBr_6.

	Cs_4SnBr_6		
Temperature (K)	272.98 (10)	199.99 (10)	100.00 (10)
Formula Weight	1129.79	1129.77	1129.77
Crystal System	trigonal	trigonal	trigonal
Space Group	*R*-3*c*	*R*-3*c*	*R*-3*c*
a (Å)	13.6687 (3)	13.6191 (2)	13.5598 (2)
c (Å)	17.2597 (5)	17.2184 (4)	17.1628 (3)
γ/°	120	120	120
Volume ($Å^3$)	2792.67 (16)	2765.80 (10)	2732.91 (9)
F(000)	2880.0	2880.0	2880
ρ_{calc} (g cm^{-3})	4.031	4.070	4.119
Radiation	Cu *K*α (λ = 1.54184 Å)	Cu *K*α (λ = 1.54184 Å)	Cu *K*α (λ = 1.54184 Å)
2θ for data collection (°)	12.694–159.126	12.73–158.642	12.776–159.604
μ (mm^{-1})	85.81	86.644	87.687
Crystal Size (mm^3)	0.047 0.037 0.025	0.047 0.037 0.025	0.047 0.037 0.025
Index Ranges	-17 ≤ h ≤ 16 -17 ≤ k ≤ 17 -21 ≤ l ≤ 21	-12 ≤ h ≤ 17 -17 ≤ k ≤ 17 -21 ≤ l ≤ 21	-13 ≤ h ≤ 17 -17 ≤ k ≤ 15 -21 ≤ l ≤ 21
Reflections Collected	19422	14101	14021
Independent Reflections	683 [R_{int} = 0.0678, R_{sigma} = 0.0155]	675 [R_{int} = 0.0568, R_{sigma} = 0.0152]	667 [R_{int} = 0.0601, R_{sigma} = 0.0166]
Data/restraints/para-meters	683/0/19	675/0/19	667/0/19
Goodness-of-fit on F^2	1.164	1.255	1.124
Final R indexes [I>=2σ (I)]	R_1 = 0.0242 wR_2 = 0.0596	R_1 = 0.0243 wR_2 = 0.0648	R_1 = 0.0257 wR_2 = 0.0678
Final R indexes [all data]	R_1 = 0.0244 wR_2 = 0.0596	R_1 = 0.0245 wR_2 = 0.0650	R_1 = 0.0258 wR_2 = 0.0678
Largest diff. peak/hole (e Å-3)	0.70/-1.79	0.76/-1.54	1.03/-1.37

The lattice parameters were determined to be larger than those previously reported[4] with *a* = *b* = 13.6687(3) and *c* = 17.2597(5) at 273 K but in close agreement with recent computational predictions.[5]

Table S4. Fractional atomic coordinates and equivalent isotropic displacement parameters ($Å^2×10^3$) for Cs_4SnBr_6 at 273 K.

Atom	Wyckoff Symbol	*X*	*y*	*z*	U(eq)[a]
Cs1	*18e*	0.62487(3)	0	1/4	30.40(15)
Cs2	*6a*	0	0	1/4	41.6(2)
Sn1	*6b*	0	0	0	18.38(18)
Br1	*36f*	0.69510 (5)	0.52439 (5)	0.23286 (3)	31.33(17)

[a] U_{eq} is defined as 1/3 of the trace of the orthogonalised U_{IJ} tensor.

Table S5. Anisotropic displacement parameters ($Å^2×10^3$) for Cs_4SnBr_6 at 273 K.

Atom	U11	U22	U33	U23	U13	U12
Cs1	30.0(2)	26.4(2)	33.6(3)	-5.37(16)	-2.69(8)	13.19(12)
Cs2	52.6(3)	52.6(3)	19.6(4)	0	0	26.29(17)
Sn1	18.8(2)	18.8(2)	17.5(3)	0	0	9.41(11)
Br1	34.8(3)	32.0(3)	31.4(3)	2.2(2)	0.2(2)	19.8(2)

[a] The anisotropic displacement factor exponent takes the form: $-2\pi^2[h^2a^{*2}U_{11}+2hka^*b^*U_{12}+\ldots]$.

Table S6. Fractional atomic coordinates and equivalent isotropic displacement parameters ($Å^2×10^3$) for Cs_4SnBr_6 at 200 K.

Atom	Wyckoff Symbol	*x*	*Y*	*z*	U(eq)[a]
Cs1	*18e*	0.62475 (3)	0	1/4	20.21(16)
Cs2	*6a*	0	0	1/4	27.8(2)
Sn1	*6b*	0	0	0	12.06(19)
Br1	*36f*	0.69512 (5)	0.52482 (5)	0.23270 (3)	21.26(18)

[a] U_{eq} is defined as 1/3 of the trace of the orthogonalised U_{IJ} tensor.

Table S7. Anisotropic displacement parameters ($Å^2×10^3$) for Cs_4SnBr_6 at 200 K.

Atom	U11	U22	U33	U23	U13	U12
Cs1	20.1(2)	17.8(2)	21.9(3)	-3.56(15)	-1.78(8)	8.89(12)
Cs2	35.5(3)	35.5(3)	12.6(4)	0	0	17.73(16)
Sn1	12.5(2)	12.5(2)	11.2(4)	0	0	6.25(12)
Br1	23.7(3)	21.8(3)	21.1(3)	1.5(2)	0.2(2)	13.5(2)

[a] The Anisotropic displacement factor exponent takes the form: $-2\pi^2[h^2a^{*2}U_{11}+2hka^*b^*U_{12}+\ldots]$.

Table S8. Fractional atomic coordinates and equivalent isotropic displacement parameters ($Å^2×10^3$) for Cs_4SnBr_6 at 100 K.

Atom	Wyckoff Symbol	x	y	z	U(eq)[a]
Cs1	*18e*	0.62455 (3)	0	1/4	8.67(17)
Cs2	*6a*	0	0	1/4	12.3(2)
Sn1	*6b*	0	0	0	4.9(2)
Br1	*36f*	0.69516 (4)	0.52533 (4)	0.23256 (3)	9.54(18)

[a] U_{eq} is defined as 1/3 of of the trace of the orthogonalised U_{IJ} tensor.

Table S9. Anisotropic displacement parameters ($Å^2×10^3$) for Cs_4SnBr_6 at 100 K.

Atom	U11	U22	U33	U23	U13	U12
Cs1	8.5(2)	7.5(2)	9.7(3)	-1.69(14)	-0.85(7)	3.76(12)
Cs2	15.7(3)	15.7(3)	5.6(4)	0	0	7.84(14)
Sn1	5.0(3)	5.0(3)	4.7(4)	0	0	2.49(13)
Br1	10.2(3)	9.8(3)	9.9(3)	0.65(18)	0.18(19)	6.0(2)

[a] The Anisotropic displacement factor exponent takes the form: $-2\pi^2[h^2a^{*2}U_{11}+2hka^*b^*U_{12}+\ldots]$.

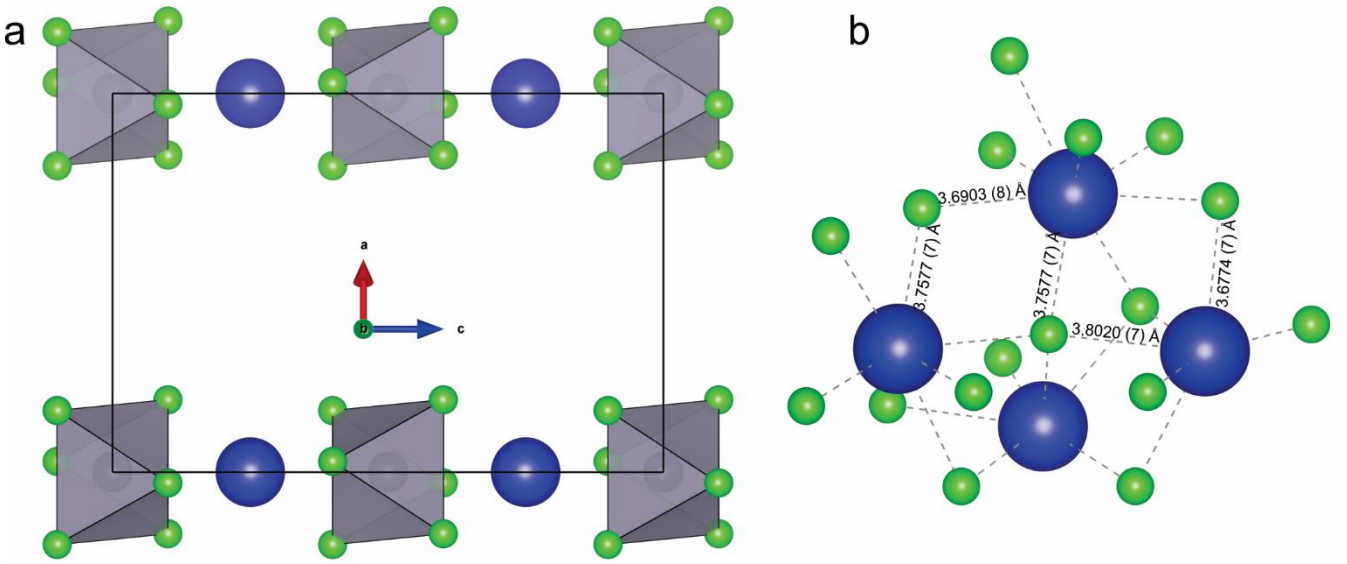

Figure S3. Distinct crystallographic positions of Cs. Views of the Cs_4SnBr_6 structure demonstrating the two distinct crystallographic positions of Cs within the structure. (a) Cs(2) cations are located between $[SnBr_6]^{4-}$ octahedra in six-fold coordination with an average Cs-Br bond length of 3.5520 (3) Å. The Sn-Sn distance along the c-axis is 8.6299 (3) Å. (b) Cs(1) is found between the columns formed by $[SnBr_6]^{4-}$ octahedra and Cs(2). It is in an eight-coordinate position with Cs-Br bond lengths ranging from 3.6774 (7) Å to 3.8020 (7) Å.

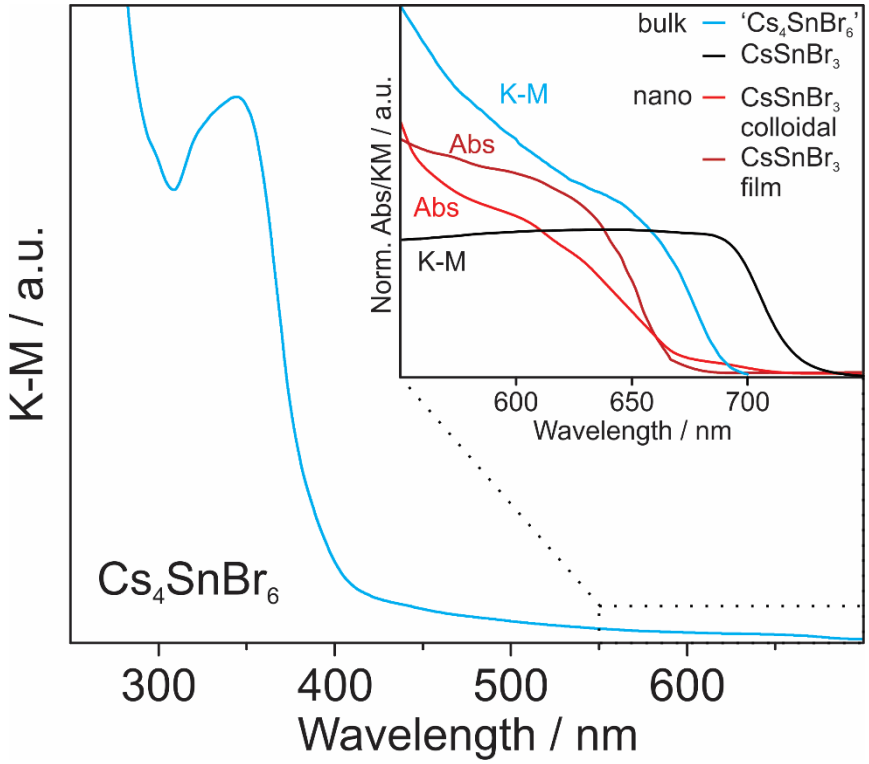

Figure S4. Absorption (Kubelka-Munk, or K-M in the Figure) spectra of Cs_4SnBr_6. The absorption spectrum demonstrates an absorption edge that ends at roughly 400 nm. (Inset) The tail observed at longer wavelengths is expanded and a shoulder at 670 nm is observed. This shoulder likely results from an impurity of $CsSnBr_3$ that, although too small (in amount and in size) to be measurable by XRD, slightly discolours the otherwise white powder giving it an off-white appearance. This is plotted in comparison to bulk and nano-crystalline $CsSnBr_3$. The colloidal nanocrystals of $CsSnBr_3$, plotted in red, are reported as being 10.7 nm ± 6.4 nm in diameter and these exhibit the most blue absorption edge in agreement with their size (data taken from Ref.[6]) Furthermore, films prepared from $CsSnBr_3$ nanocubes also have absorption edges that are blueshifted from that of bulk $CsSnBr_3$ and near to that of colloidal $CsSnBr_3$ NCs (data taken from Ref.[7]). Given this optical data, the tail and shoulder observed in the absorption spectrum of Cs_4SnBr_6 are ascribed to $CsSnBr_3$.

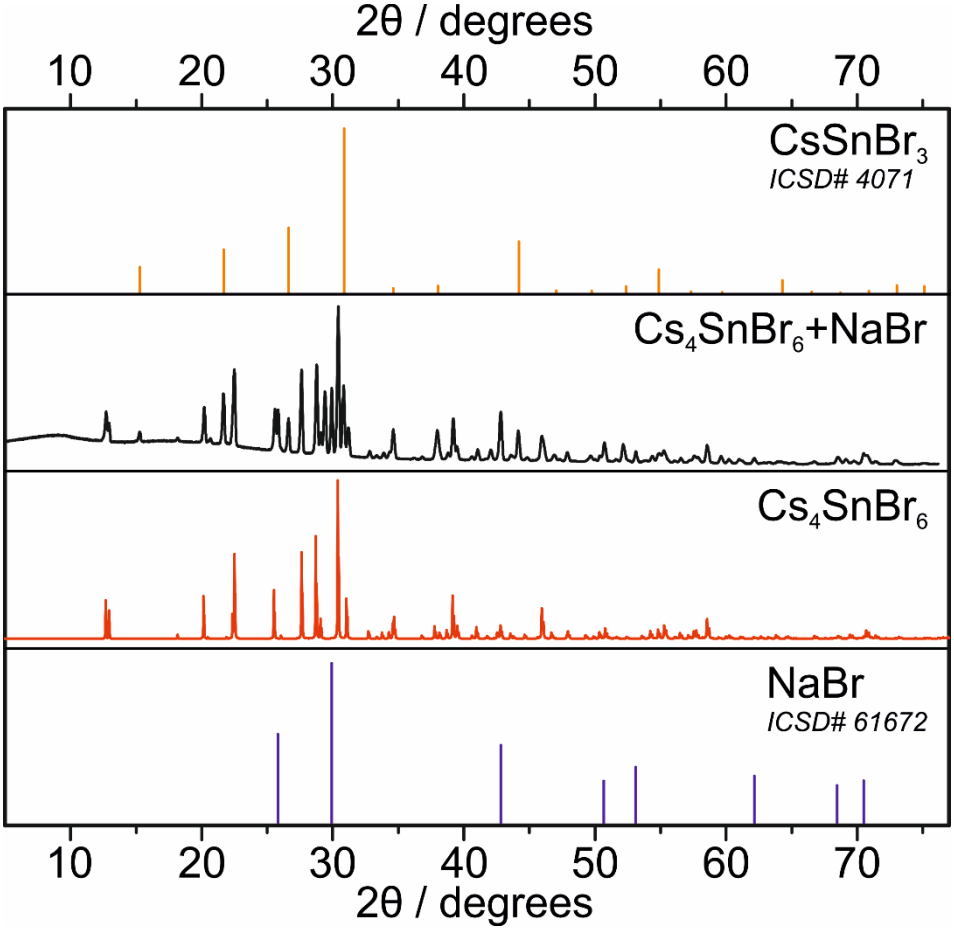

Figure S5. Substitution with Na. Cations smaller than K^+ do not substitute Cs^+ in Cs_4SnBr_6. The addition of Na resulted in a mixture of Cs_4SnBr_6, $CsSnBr_3$ (ICSD# 4071), CsBr (not shown), and NaBr (ICSD# 61672).

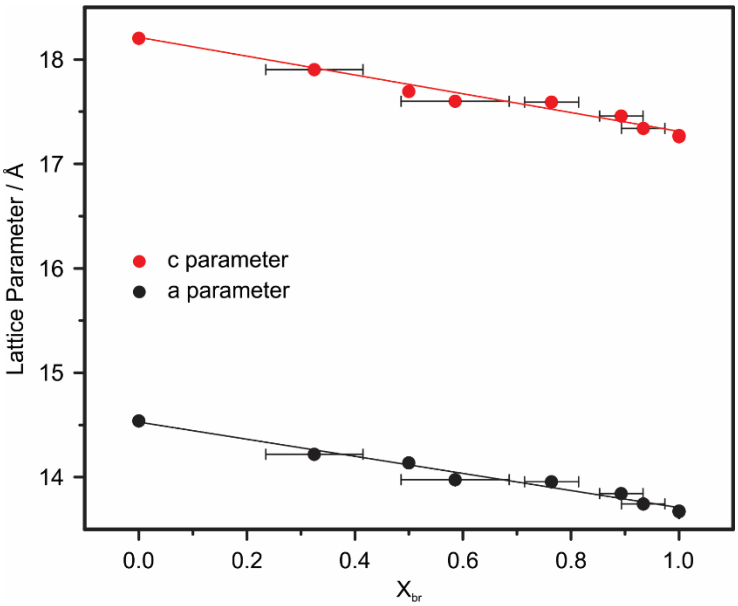

Figure S6. Bromide and iodide substitution. The substitution of bromide for iodide results in a linear change in the a and c lattice parameters. This is in agreement with Vegard's law and suggests a solid solution exists between Br and I on these general positions. The R^2 value for the linear fit of lattice parameter vs. molar fraction of bromide is 0.98 for both the *a* and *c* parameters.

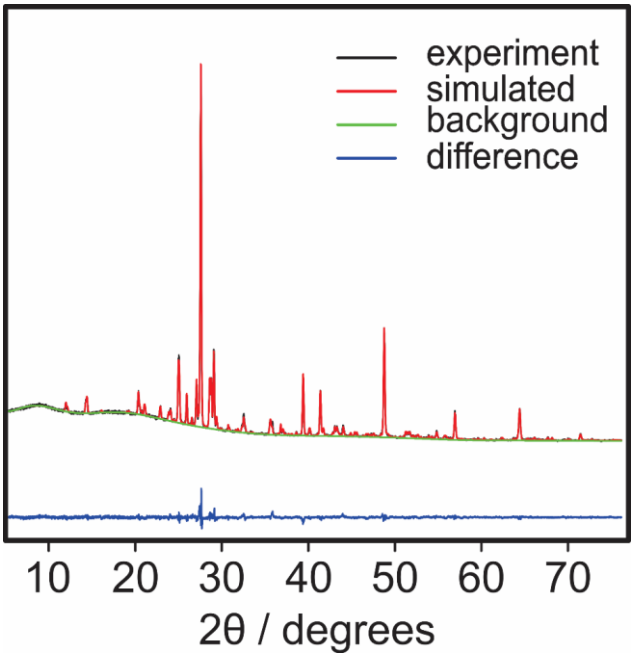

Figure S7. Refinement of Cs_4SnI_6. The crystal structure of Cs_4SnI_6 was determined through Rietveld refinement using GSAS and EXPGUI.

Table S10. Refinement of Cs_4SnI_6.

Sample	**Cs_4SnI_6**
Temperature	298 K
Formula Weight	1411.73
Crystal System	trigonal
Space Group	*R-3c*
Color	Black
a (Å)	14.5315 (4)
c (Å)	18.1571 (8)
Volume (Å3)	3028.52
Z	6.0
F(000)	3528
ρ_{calc} (g cm^{-3})	4.222
Radiation	Cu Kα (λ = 1.54184 Å)
2θ for data collection (°)	5.01–75.00
2θ step (°)	0.01
Data/restraints/para-meters	7000/0/43
Rp	0.028
Rwp	0.037
Rexp	0.029
Goodness-of-fit on F2	0.05787
χ^2	1.638
(Δ/σ)max	0.06

Table S11. Fractional atomic coordinates and isotropic or equivalent isotropic displacement parameters (Å^2) for Cs_4SnI_6.

Atom	**Wyckoff Symbol**	**X**	**Y**	**Z**	**Uiso*/Ueq**
Sn1	*6b*	0	0	0	0.0729 (15)*
Cs1	*18e*	0.3787 (4)	0	1/4	0.0729 (15)*
Cs2	*6a*	0	0	1/4	0.0729 (15)*
I1	*36f*	0.1404 (4)	0.5044 (5)	0.0641 (2)	0.0729 (15)*

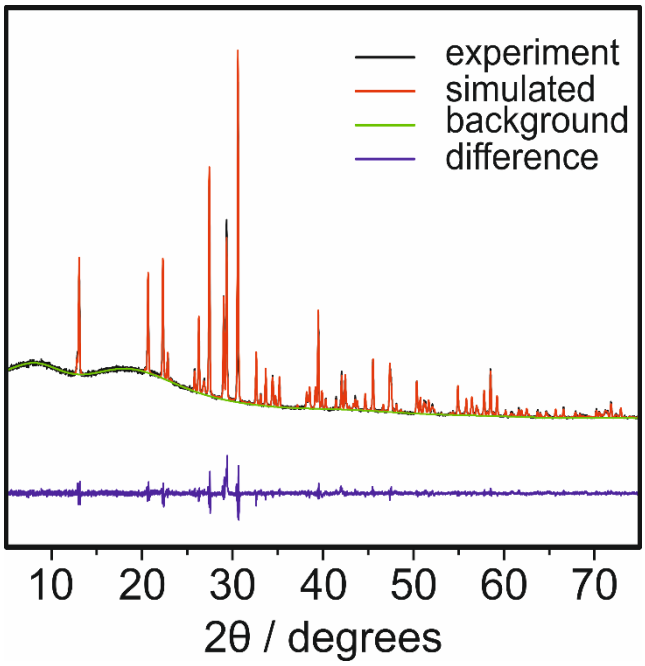

Figure S8. Refinement of $Cs_{3.2}K_{0.8}SnBr_6$. The crystal structure of $Cs_{3.2}K_{0.8}SnBr_6$ was determined through Rietveld refinement using GSAS and EXPGUI.

Table S12. Refinement of $Cs_{3.2}K_{0.8}SnBr_6$.

Sample	**$Cs_{3.20}K_{0.80}SnBr_6$**
Temperature	298 K
Formula Weight	1054.92
Crystal System	trigonal
Space Group	*R*-3*c*
Color	colorless
a (Å)	13.79233 (8)
c (Å)	16.45368 (17)
Volume (Å^3)	2710.62 (3)
Z	6.0
F(000)	2708
ρ_{calc} (g cm^{-3})	3.877
Radiation	Cu $K\alpha$ (λ = 1.54184 Å)
2θ for data collection (°)	5.00–75.99
2θ step (°)	0.01
Data/restraints/para-meters	7100/0/24
R_p	0.033
R_{wp}	0.049
R_{exp}	0.030
R(F^2)	0.07058
χ^2	2.560
$(\Delta/\sigma)_{max}$	0.68

Table S13. Fractional atomic coordinates and isotropic or equivalent isotropic displacement parameters (Å^2) for $Cs_{3.2}K_{0.8}SnBr_6$.

Atom	**Wyckoff Symbol**	**X**	**Y**	**Z**	**Uiso*/Ueq**	**Occ. (<1)**
Cs1	*18e*	0.37804 (11)	x	3/4	0.05625*	
Sn2	*6b*	1/3	2/3	2/3	0.05625*	
Cs3	*6a*	2/3	1/3	0.58333	0.05625*	0.20243
Br4	*36f*	0.36230 (15)	0.50857 (16)	0.55817 (8)	0.05625*	
K5	*6a*	2/3	1/3	0.58333	0.05625*	0.79755

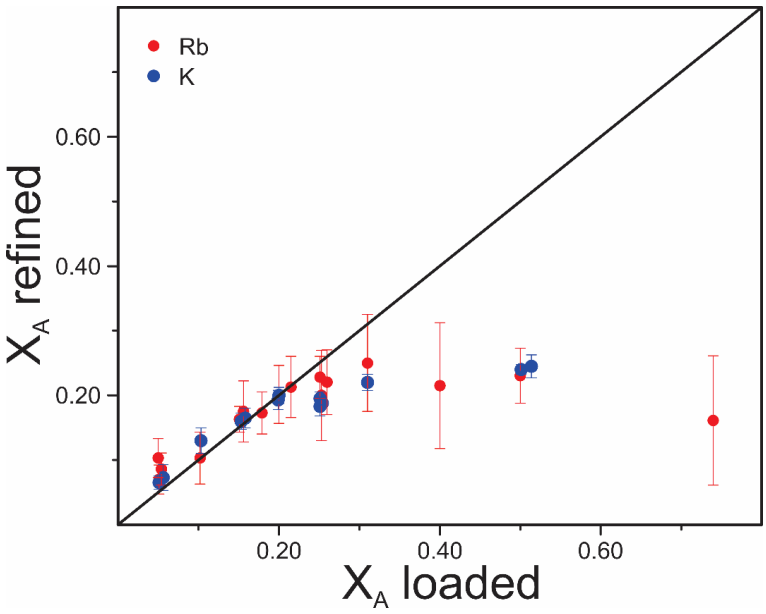

Figure S9. Limited A-site substitution. The substitution of the A-site in Cs_4SnBr_6 does not exceed 25% with either Rb^+ or K^+. Much higher loadings tend to yield samples with greater amounts of impurities such as the darkly colored $CsSnBr_3$.

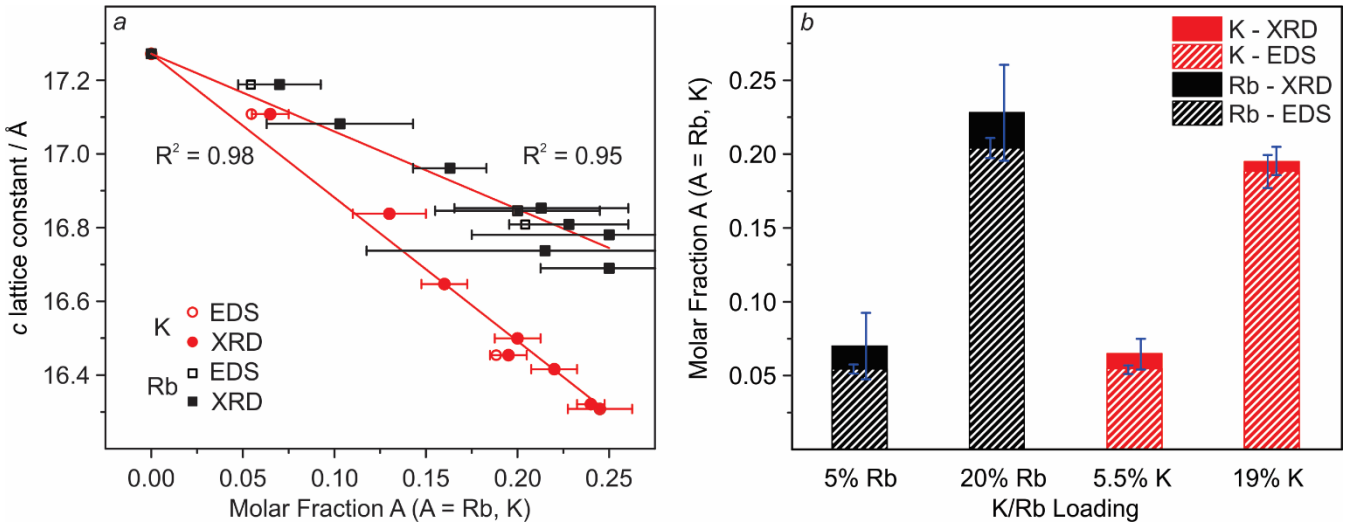

Figure S10. Expanded view of the *c*-lattice parameter's dependence on A-site occupancy. (a) For both K- and Rb- substitution, a linear change in the *c*-lattice parameter with the molar fraction of K and Rb ions is observed with R^2 values of 0.98 and 0.95, respectively. Error bars represent the standard uncertainty as calculated from the Rietveld refinement by GSAS. The larger error bars for the samples with Rb-substitution come as a result of the smaller differences in electron density between Cs and Rb than between Cs and K. (b) The composition as determined by EDS is compared with that determined by Rietveld refinement.

a

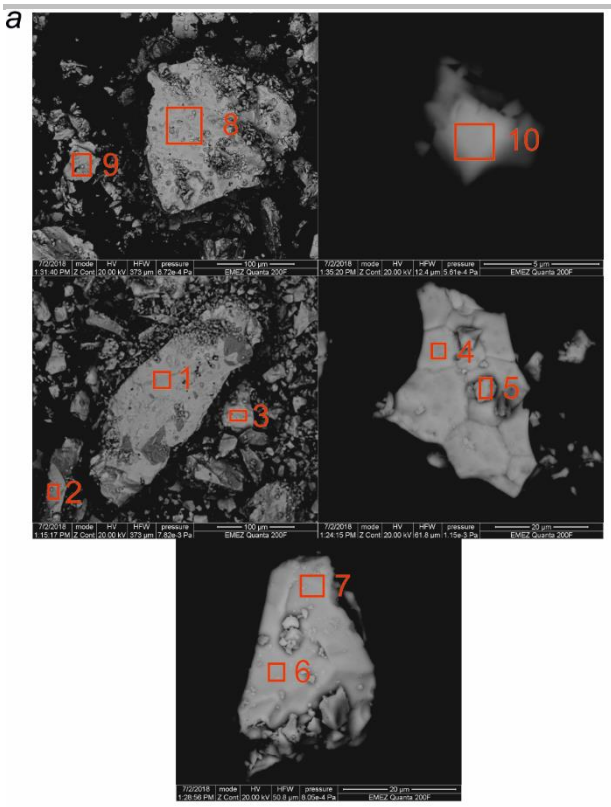

b

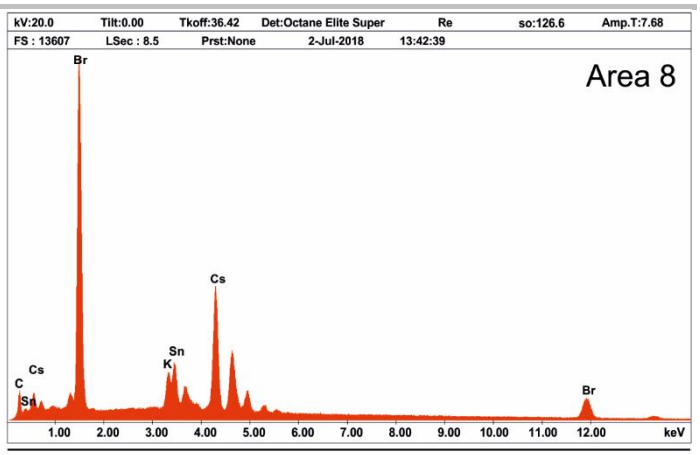

c

Area	K, wt%	K, at%	Sn, wt%	Sn, at%	Cs, wt%	Cs, at%
1	5.18	15.34	19.84	19.35	74.97	65.3
2	4.83	14.41	19.74	19.4	75.43	66.19
3	4.96	14.74	19.77	19.38	75.27	65.88
4	5.11	15.14	19.95	19.48	74.95	65.38
5	5.92	17.28	19.06	18.32	75.02	64.4
6	5.06	15.02	20.17	19.72	74.77	65.26
7	5.18	15.34	20.61	20.09	74.2	64.58
8	5.31	15.67	19.85	19.31	74.84	65.02
9	4.79	14.32	17.95	17.68	77.27	67.99
10	5.05	14.99	19.47	19.06	75.48	65.96

Figure S11. SEM and EDS of $Cs_{3.2}K_{0.8}SnBr_6$. (a) SEM images obtained from $Cs_{3.2}K_{0.8}SnBr_6$. (b) The EDS spectrum measured from the region marked with the number 8. (c) The K, Sn, and Cs weight percent (wt%) and atomic percent (at%) as measured in 10 regions (individually marked in subfigure a). This same process was repeated for all 4 points presented in Fig. S10.

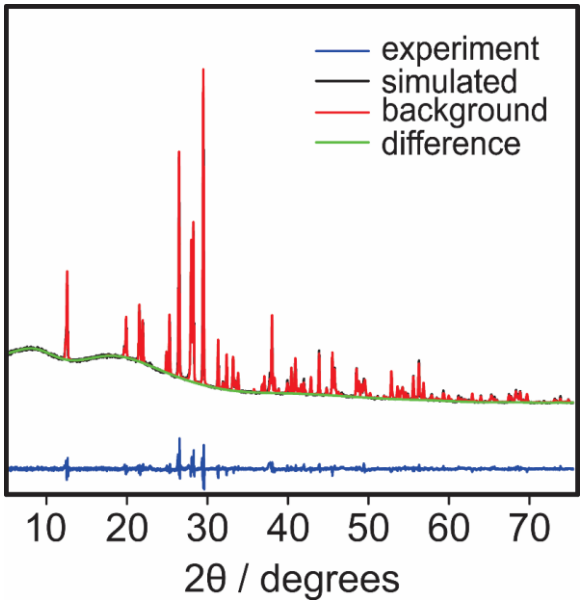

Figure S12. Refinement of $Cs_{3.2}K_{0.8}SnBr_3I_3$. The crystal structure of $Cs_{3.2}K_{0.8}SnBr_3I_3$ was determined through Rietveld refinement using GSAS and EXPGUI.

Table S14. Refinement of $Cs_{3.2}K_{0.8}SnBr_3I_3$.

Sample	**$Cs_{3.28}K_{0.72}SnBr_{2.85}I_{3.15}$**
Temperature	298 K
Formula Weight	1209.61
Crystal System	trigonal
Space Group	*R-3c*
Color	pale yellow
a (Å)	14.28389 (9)
c (Å)	17.11201 (19)
Volume (Å3)	3023.604 (33)
Z	6.0
F(000)	3064
ρ_{calc} (g cm^{-3})	3.986
Radiation	Cu Kα (λ = 1.54184 Å)
2θ for data collection (°)	5.01–75.44
2θ step (°)	0.01
Data/restraints/para-meters	7045/0/7
Rp	0.029
Rwp	0.044
Rexp	0.024
R(F2)	0.09110
χ^2	3.349
(Δ/σ)max	0.03

Table S15. Fractional atomic coordinates and isotropic or equivalent isotropic displacement parameters (Å^2) for $Cs_{3.2}K_{0.8}SnBr_3I_3$.

Atom	Wyckoff Symbol	X	Y	Z	Uiso*/Ueq	Occ. (<1)
Cs1	*18e*	0.38179 (12)	0	1/4	0.0607 (4)*	
Sn2	*6b*	0	0	0	0.0607 (4)*	
Cs3	*6a*	0	0	1/4	0.0607 (4)*	0.27543
Br4	*36f*	0.14407 (12)	0.50868 (14)	0.05804 (7)	0.0607 (4)*	0.47572
K5	*6a*	0	0	1/4	0.0607 (4)*	0.72457
I6	*36f*	0.14406 (12)	0.50867 (14)	0.05804 (7)	0.0607 (4)*	0.52428

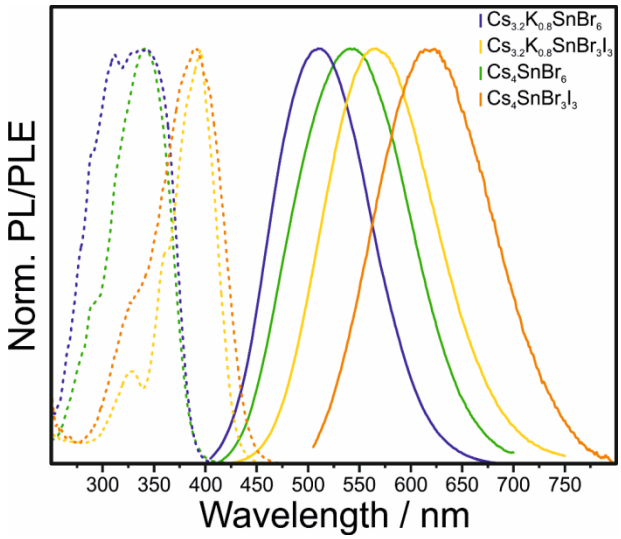

Figure S13. Room temperature PL spectra of samples measured at Low T. PL and PLE spectra of the four samples that were used for temperature dependent PL measurements down to 6 K. These spectra were measured at room temperature.

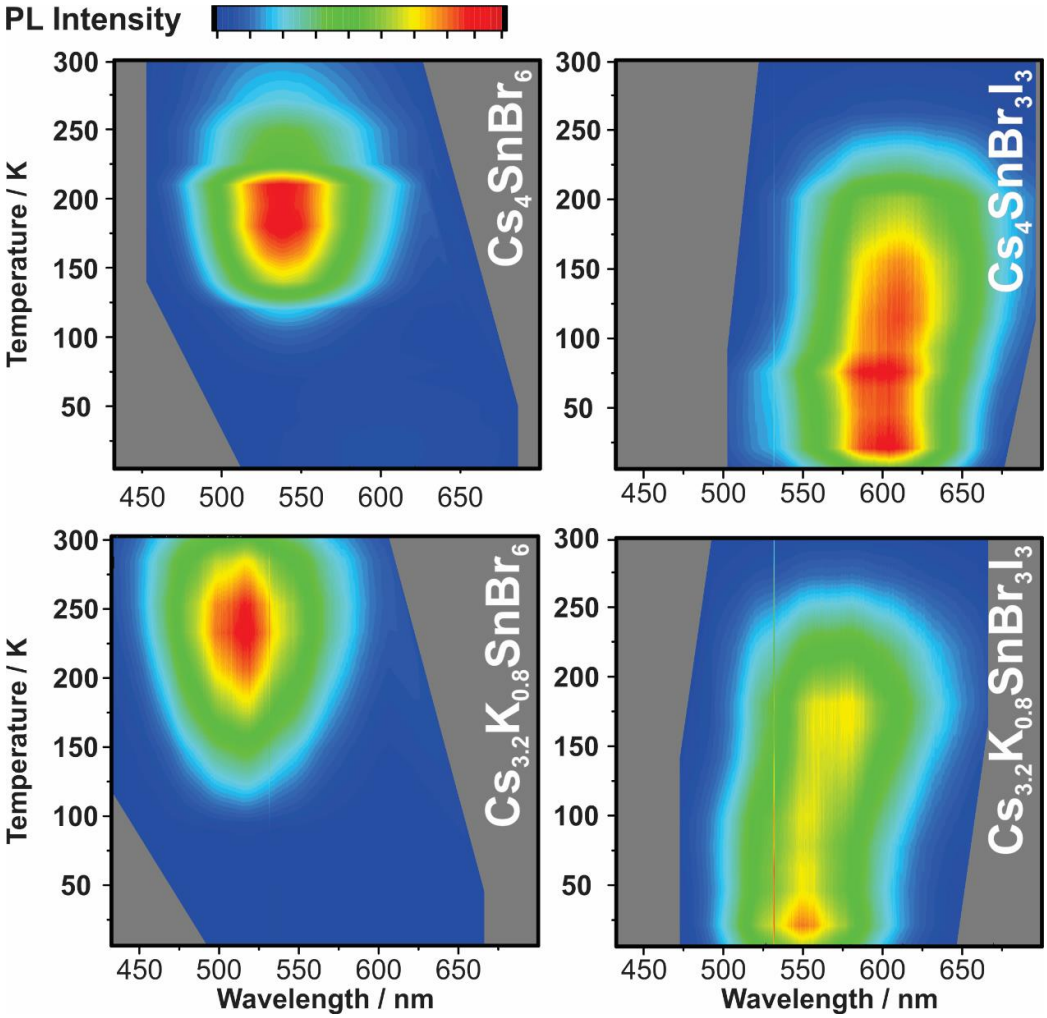

Figure S14. Temperature dependent PL spectra. Temperature dependent PL spectra collected from 300 K to 6 K with a 355 nm excitation laser. The composition which corresponds to the spectra is written in the right corner of each graph.

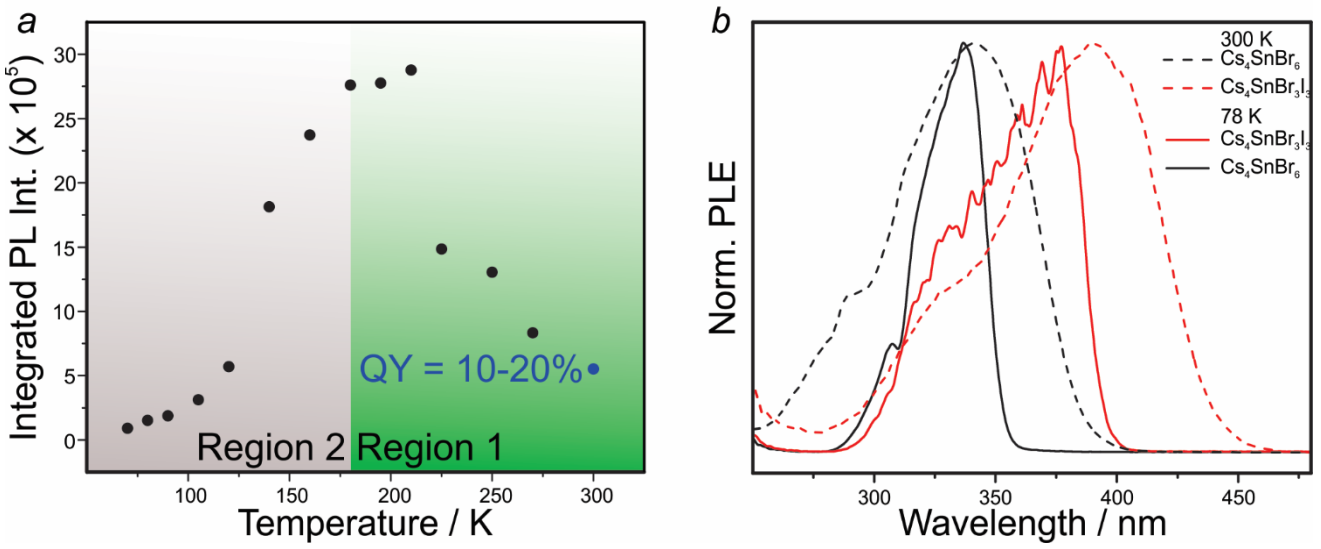

Figure S15. Temperature dependence of PL intensity and temperature dependent excitation spectra. (a) The integrated PL intensity of Cs_4SnBr_6 plotted against temperature indicates that there are two regimes present: region 1 and region 2. Region 1 involves a PL increase, and is related to an increasing QY since any decrease in absorption in Region 1 is still met with an increase in the PL intensity. Region 2, however, demonstrates a loss of PL with decreasing temperature. This loss is explained by (b) PLE measured at 78 K. As the temperature decreases, it is observed that the excitation peak narrows and that the peak position slightly blue shifts. These two effects inhibit the material from being efficiently excited with a 355 nm laser. The slight blue shift in the PLE can be explained by the lattice contraction observed in Table S3. Furthermore, the average Sn-Br distance decreases from 2.9939 (7) Å to 2.9854 (6) Å when cooled from 273 K to 100 K.

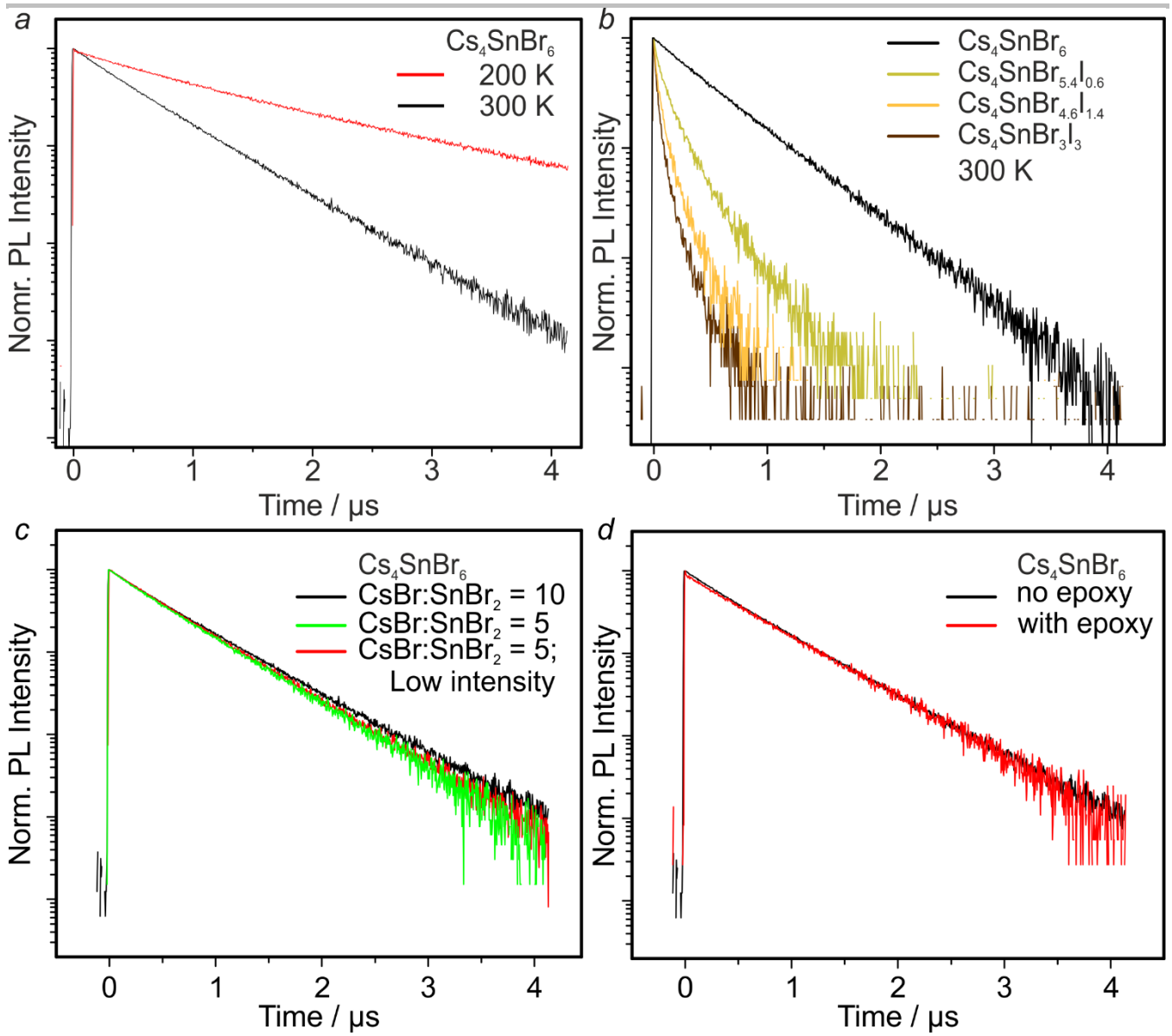

Figure S16. Time-resolved PL spectra. (a) Changing temperature results in a lengthening of the PL lifetime. (b) The addition of iodide shortens the average PL lifetime. (c) Preparing Cs_4SnBr_6 with different $CsBr:SnBr_2$ ratios yields materials with equivalent average lifetimes. Furthermore, the PL lifetime is intensity-independent. (d) Encapsulation with a UV-curable epoxy also does not affect the measured PL lifetime.

2.2 Computational details

Calculations were carried out at the Density Functional Theory level as implemented in the cp2k quantum chemistry code. A single 1x1x1 unit cell containing 66 atoms was constructed for all materials involved. A mixed plane-wave and Gaussian basis set approach was used to describe the wave function and electronic density, respectively. The kinetic energy cutoff of the plane-wave basis was set to 400 Rydberg, while a double-ζ basis set plus polarization functions was employed to describe the molecular orbitals. Density of States (DOS), emission and excitation energies were calculated using Perdew-Burke-Ernzerhof (PBE) exchange-correlation functional. Scalar relativistic effects have been accounted for by using effective core potential functions in the basis set. Spin-orbit coupling effects were not included. The optical excitation and emission energies were obtained by computing the total energy differences between the ground state and excited-state structures, at the ground state and excited state geometries respectively. Excited state geometry optimizations were performed with unrestricted Kohn-Sham calculations for a triplet multiplicity with fixed lattice parameters, optimized for the ground state geometry. We assume that the triplet energy and structure are qualitatively similar to the excited state singlet. Calculations with lattice relaxation for the ground state geometry optimization were performed to account for statistical disorder in the experimental crystal structures. External pressure applied for cell optimization was 100 bar. Atomic coordinates were optimized until the force reached 0.023 eV/ Å. Calculation for structures at different temperatures were performed without geometry relaxation on the lattices obtained from single crystal X-ray diffraction (Table S3-9) In general, lattice relaxation facilitates the convergence of the excited state geometry but underestimates the real emission and excitation energies (Table S16).

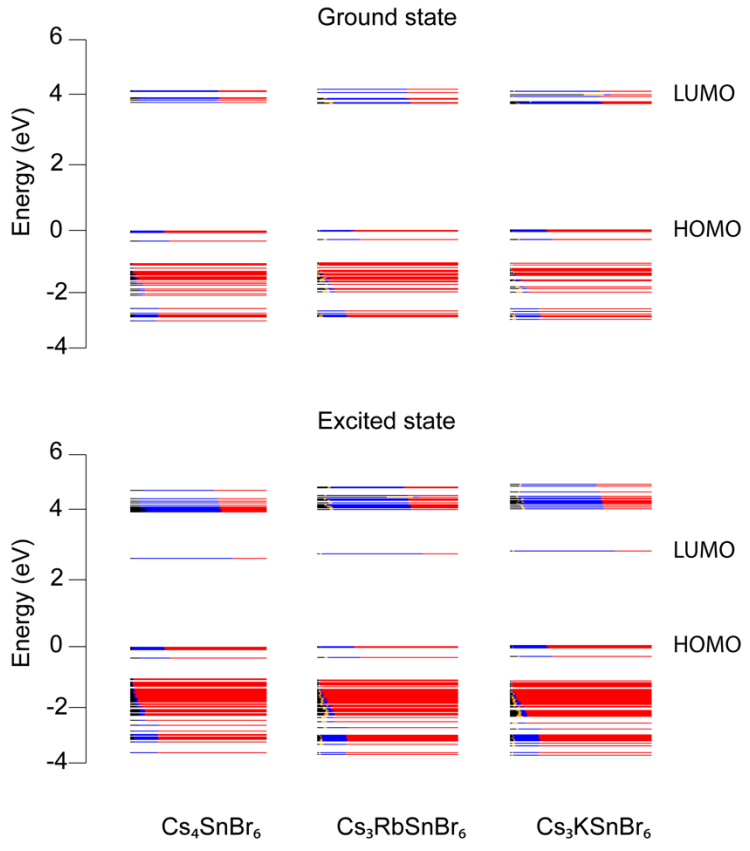

Figure S17: Frontier orbitals (HOMO and LUMO) for ground and excited states of A_4SnBr_6. Color-code: black – Cs, orange – Rb/K, blue – Sn, red – Br. Molecular orbitals for ground and excited state obtained from single-point calculations on optimized ground and excited state geometry. The values of HOMO-LUMO gap from single-point calculations are not reliable and are omitted. The LUMO in excited state comprises exclusively Sn-5p and Br-4p orbitals from distorted $SnBr_6$ octahedron As discussed, the contribution of A-site cation to the band edge is negligible (black and orange). HOMO is comprised of Sn s-orbitals and Br p-orbitals, whereas Sn-p orbitals and Br p-orbitals contribute to the LUMO.

Table S16. Comparison of calculated energies (eV) for three different approaches: lattice fixed at experimental values, lattice optimization for the ground state only, and the lattice optimized for both ground and excited states; g-e – difference in total energies of ground and excited states.

	No lattice optimization		Lattice optimization - ground state		Lattice optimization - both states	
	g-e (eV)	Emission (eV)	g-e (eV)	Emission (eV)	g-e (eV)	Emission (eV)
Cs_4SnBr_6	2.9	2.3	2.9	2.25	2.9	2.15
$Cs_3RbSnBr_6$	3.0	2.4	2.9	2.3	2.9	2.2
Cs_3KSnBr_6	3.0	2.4	2.9	2.4	2.9	2.3

Table S17. Bond distances (Å) for axial and equatorial Sn-Br bonds in the optimized ground and excited state geometries.

Compound	Ground state		Excited state	
	Axial (Å)	Equatorial (Å)	Axial (Å)	Equatorial (Å)
Cs_4SnBr_6	3.049	3.049	3.658	2.88
$Cs_3RbSnBr_6$	3.042	3.042	3.603	2.88
Cs_3KSnBr_6	3.035	3.035	3.567	2.88

As a general trend, the axial Sn-Br bond is elongated depending on the cation, whereas equatorial bond decreases to the same value regardless the composition.

Table S18. Bond distances (Å) for excited and ground state, calculated emission and absorption energies for Cs_4SnBr_6 at different temperatures (273, 200, and 100 K).

Temperature (K)	c/a ratio	Axial bond (Å)		Equatorial bond (Å)		Calculated	Calculated
		Ground	Excited	Ground	Excited	Emission (eV)	Absorption (eV)
273	1.263	3.000	3.562	3.000	2.880	2.33	3.55
200	1.264	2.990	3.550	2.990	2.881	2.34	3.54
100	1.266	2.985	3.538	2.985	2.878	2.34	3.53

The relative change in Sn-Br bond distance is much smaller than for different compositions. The calculations were performed with lattice parameters fixed at experimental values and relaxing only atomic positions.

3. REFERENCES

[1] G. M. Sheldrick, *Acta Cryst.* **2008**, *64*, 112-122.
[2] O. V. Dolomanov, L. J. Bourhis, R. J. Gildea, J. A. K. Howard, H. Puschmann, *J. Appl. Cryst.* **2009**, *42*, 339-341.
[3] a) B. H. Toby, R. B. Von Dreele, *J. Appl. Cryst.* **2013**, *46*, 544-549; b) B. H. Toby, *J. Appl. Cryst.* **2001**, *34*, 210-213.
[4] R. H. Andrews, S. J. Clark, J. D. Donaldson, *J. Chem. Soc., Dalton Trans.* **1983**, 767-770.
[5] M. Hu, C. Ge, J. Yu, J. Feng, *J. Phys. Chem. C* **2017**, *121*, 27053-27058.
[6] T. C. Jellicoe, J. M. Richter, H. F. Glass, M. Tabachnyk, R. Brady, S. E. Dutton, A. Rao, R. H. Friend, D. Credgington, N. C. Greenham, M. L. Bohm, *J. Am. Chem. Soc.* **2016**, *138*, 2941-2944.
[7] A. Wang, Y. Guo, F. Muhammad, Z. Deng, *Chem. Mater.* **2017**, *29*, 6493-6501.